Selective Correlation Detection of Photonically Generated Ultrawideband RF Signals

Ingrid S. Lin, *Student Member, IEEE*, and Andrew M. Weiner, *Fellow, IEEE*

***Abstract*—We demonstrate hardware auto/cross-correlation measurements of photonically generated ultrawideband (UWB) RF burst waveforms in the 3–10 GHz range. Full delay dependent correlation studies with matched waveform pairs reveal correlation peaks $\sim$15 dB above those obtained with nonmatching sets of waveforms. The possibility of real-time correlation detection is also explored, as are correlation measurements of waveforms that are transmitted over a short line-of-sight wireless link. With waveforms modified to precompensate for antenna dispersion, 7 dB correlation contrast between matched and nonmatched waveform pairs is obtained. Our results suggest hardware correlation detection as a possibility for processing of arbitrary waveforms in an Ultra-wideband (UWB) receiver.**

***Index Terms*—Broadband correlation, optical pulse shaping, ultrawideband (UWB).**

I. Introduction

CURRENT interest in ultrawideband (UWB) wireless systems for communications [1], imaging systems and ground penetrating radar motivates novel techniques for arbitrary electrical waveform generation (AWG). Our group and others [2]–[7] have reported studies demonstrating the use of optical pulse shaping followed by optical-to- electrical conversion for generation of arbitrary burst electrical waveforms with instantaneous bandwidths (BW) spanning (or in some cases significantly exceeding) the UWB frequency band (3.1–10.6 GHz). Recently, commercial electronic arbitrary waveform technology has also advanced to > 5 GHz instantaneous bandwidth [8], which is sufficient, if appropriately upconverted, to cover much of the UWB band. Optical techniques retain advantages such as possibility of reaching much higher instantaneous bandwidth and compatibility with remoting applications. The advent of UWB arbitrary waveform generation, using either photonic or electronic solutions, allows new capabilities, such as antenna dispersion precompensation, to be applied on the transmitter end for UWB wireless studies [9]. However, to fully exploit arbitrary RF waveforms for UWB, new processing approaches are needed at the receiver, since conventional analog-to-digital conversion and digital signal processing are inadequate to handle the full UWB band.

One possibility is to perform correlation processing in hardware. Studies of RF correlators aiming at the UWB frequency band (3.1–10.6 GHz) are important for exploiting full UWB systems potential [10]. Examples of UWB correlators include a radio-frequency (RF) integrated circuit implementation [11] with 600-MHz operating frequency and SAW (surface acoustic wave) filters with center frequency 3.63 GHz and BW $\sim$1 GHz [12]. However, none of the abovementioned methods provides correlation solutions covering the full UWB bandwidth.

Here we report the use of broadband RF mixers for correlation studies of photonically generated electrical signals spanning much of the UWB band. The concept is shown in Fig. 1(a). When two identical and synchronized (matched) signals are connected to the two mixer input ports, the mixer output taken through an appropriate low-pass filter (integrator) reaches a large output value. However, when the input signals are poorly matched (either sufficiently different or out of synchronism), the output value remains small.

In this paper, we present hardware measurement of delay-dependent correlation functions of orthogonal RF signal pairs and broadband RF waveforms. Waveforms with good autocorrelation properties (large peak-to-sidelobe ratio) are desirable for applications such as ranging. Waveform pairs or families with good cross-correlation properties (strong suppression of cross-correlation signal, preferably at all delays, in comparison to autocorrelation peaks) are of interest for applications such as UWB-CDMA [13]. In [14], we reported preliminary results with a focus on hardware autocorrelation measurements and with relatively weak (7 dB) contrast between the autocorrelation peak and its sidelobes. Here we extend our studies to consider both auto- and cross- correlation measurements, i.e., we perform correlation measurements both of matched and unmatched waveforms. By considering new waveform designs, and more precisely controlling the photonic arbitrary waveform generation, we achieve much stronger correlation contrasts (15 dB), both in auto and cross correlation. Furthermore, we demonstrate the potential for waveform selective real-time detection and include correlation measurements of waveforms transmitted over a short line-of-sight wireless link. In the case of the wireless link, the auto- to cross-correlation contrast is reduced to 7 dB as a result of reduced bandwidth of the transmitted signal.

We note that previous work in our group introduced a photonic approach to realize programmable spectral phase functions over a 20–GHz RF frequency band [15]. These systems have potential to serve as programmable RF matched filters with potential application within receivers for UWB. Another paper

Manuscript received January 30, 2008; revised May 13, 2008. Current version published October 10, 2008. This work was supported in part by the Army Research Office by Grant DAAD19-03-1-0275 and by the National Science Foundation by Grant ECCS-0701448.

The authors are with the Electrical and Computer Engineering Department, Purdue University, West Lafayette, IN 47907 USA (e-mail: ilin@purdue.edu).

Color versions of one or more of the figures in this paper area available online at http://ieeexplore.ieee.org.

Digital Object Identifier 10.1109/JLT.2008.927174

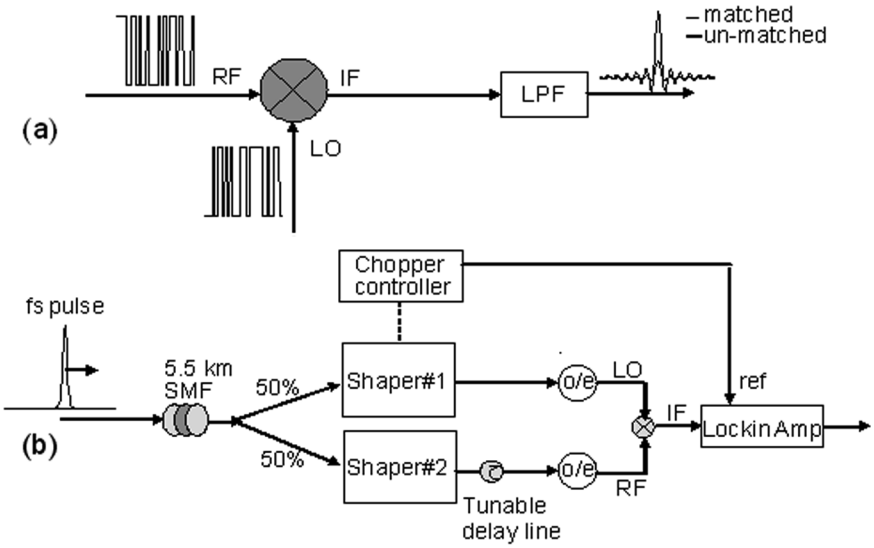

Fig. 1. (a) Conceptual illustration of RF mixer-based correlator. (b) Schematic of photonic processing UWB RF correlator.

from our group, also submitted to this Special Issue, demonstrates such matched filtering operation for the first time.

II. Experimental Apparatus

Fig. 1(b) illustrates the setup of our UWB RF correlation experiments. Highly structured RF signals are programmably generated via a photonic AWG method, details of which are given in [3], [4]. A similar photonic AWG apparatus was reported by Jalali *et al.* [5]. Other groups also showed waveform generators using fiber stretching and fiber Bragg grating-based variable optical filters followed by optical-to-electrical conversion [6], [7]. Although implemented with a specific RF AWG realization, our experiments bear on the general problem of ultrawideband electrical correlation detection using broadband electrical mixers, independent of the specific waveform generation solution employed.

Briefly, a 5.5-km single-mode optical fiber stretches femtosecond pulses from our mode-locked erbium fiber laser ($\sim$100 fs, 50-MHz repetition rate) to duration of 3 ns. Individual frequency components of the incident pulse are angularly dispersed by a diffraction grating, and focused at a 128–pixel liquid crystal modulator (LCM) array, where the spatially separated frequency components are modulated in polarization resulting in intensity modulation after a polarizing beam splitter. This allows incorporation of a large amount of structure into the optical power spectrum according to user specification. The stretched optical signals are converted to the electrical domain via a 22-GHz bandwidth photodetector. The resulting electrical waveforms represent a stretched version of the shaped optical power spectrum. Note that because the photodiodes respond only to optical power, the generated electrical waveforms are constrained to be positive definite. The resulting pedestal can be removed, at least in part, by high-pass filtering, e.g., during antenna transmission. Optical balanced detection [7] or RF balanced circuitry (e.g., rat-race 180-degree hybrid coupler) may also be employed to remove the baseband pedestal, although these are not implemented here.

In order to obtain precise control over the generated waveforms, it is important to carefully calibrate the mapping between the various pixels of the LCM array and wavelength. This is done by turning one single LCM pixel on at a time while turning the rest of the pixels off and recording the spectral peak at the output with an optical spectrum analyzer (OSA). This measurement is repeated for every pixel and for each shaper. The mapping is close to linear, but with $\sim$3.79% nonlinearity across the array. Furthermore, the nonlinearity is somewhat different for the two pulse shapers used in this paper, due to differences in their construction such as the incident angles onto the gratings. By accounting for these nonlinearities in wavelength-to-pixel mapping in the software control of the LCMs, we obtain significantly better correlation contrasts compared to our earlier preliminary study [14], where this nonlinearity was not taken into account.

A double-balanced RF mixer (Advanced Microwave part #M3301) is used as the nonlinear element needed to perform a hardware correlation. The mixer operates in frequency down-conversion mode, where a low power level RF waveform and an RF local oscillator (LO) waveform are mixed together to produce an intermediate difference frequency (IF) signal. The bandwidth is 18 GHz (4–22 GHz) for both RF and LO input ports of our mixer, and 3 GHz (0–3 GHz) for the IF output port. Accordingly, the bandwidth of the electrical mixer should be sufficient to accommodate ultrawide bandwidth signals. A 7-dBm average power is required for the LO level for proper mixer operation in a linear region. The typical conversion loss of our mixer is 6 dB. RF amplifiers are included in our setup prior to the mixer LO and RF ports to obtain sufficient signal level. In order to study the fidelity of the correlation process, we use a free-space double-path optical delay line incorporating a 20.5-cm computer controlled motorized stage. The full correlation function is obtained by scanning the optical delay of signal #2 (from the second pulse shaper) and recording the mixer output as a function of delay. The step size of the motorized stage is 0.8 mm/step, corresponding to a delay increment of 5.3 ps/step. The mixer output is sent into a lock-in amplifier

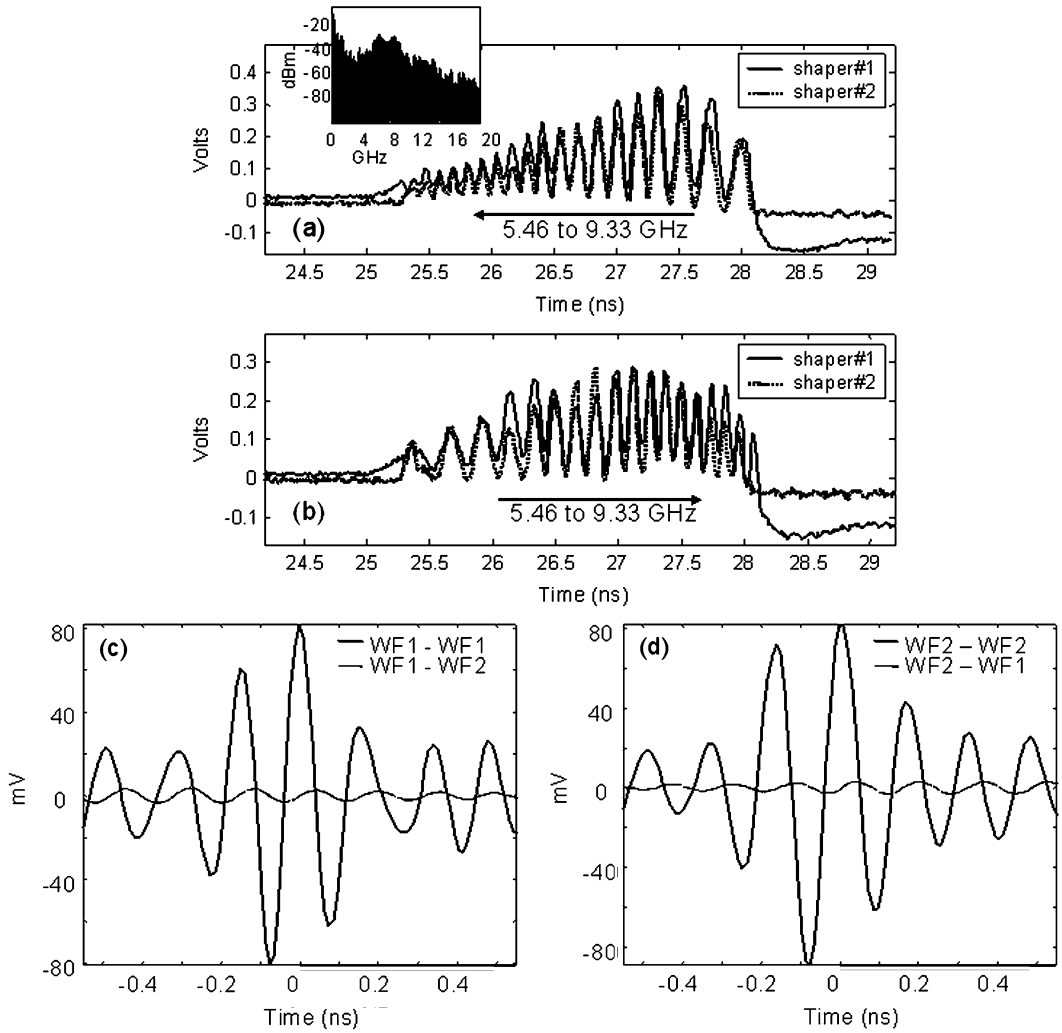

Fig. 2. Temporal waveforms of UWB linear chirped signals. (a) Downchirped waveforms, inset: RF spectrum. (b) Upchirped waveforms; Correlation traces. (c) Measured correlation traces, bold solid: matched WF1-WF1, dotted: unmatched: WF1-WF2. (d) Measured correlation traces, bold solid: matched WF2-WF2, dotted: unmatched: WF2-WF1.

with sensitivity set as 100 mV and time constant at 100 ms for recording the dc magnitude of the mixed IF output at each delay position. The recorded output constitutes the desired correlation measurement.

In additional measurements, we look at the contrast between correlation signals from matched and unmatched waveform pairs in real time (without the lock-in amplifier). We also perform an experiment with a short free-space RF link inserted in the signal path. Details of these additional experiments will be discussed later.

III. Measurement and Results

Mathematically, the mixer performs a correlation function, given by $x(t, t-\tau) = E[V_1(t) \cdot V_2(t-\tau)]$ [16]. The V_1 and V_2 denote the two input signals that are displaced by a variable delay τ. The mean value of the multiplication of two inputs then gives a correlation output x as a function of delay τ. We now present several representative RF waveforms and their correlations generated in our system.

First, we use UWB linear chirped frequency-modulated signals as shown in Fig. 2. Both downchirped (WF1, Fig. 2(a)] and upchirped [WF2, Fig. 2(b)] waveforms are considered. In each case, the peak frequency is 6.56 GHz with RF 10-dB BW from 5.46 $\sim$9.33 GHz [inset of Fig. 2(a)] filling more than half of the FCC-allocated 3.1–10.6 GHz UWB band. The generated linear chirped UWB waveforms are shown in Fig. 2(a)–(b) from both pulse shapers. The nonflat intensity envelope reflects the shape of the input optical power spectrum. In principle this can be eliminated by intensity equalization of the optical spectrum, but is not implemented in the current experiment. Care is taken to accurately measure the pixel-to-time mappings of each of the pulse shapers, so that the same chirp function may be generated from each shaper. We use opposite chirping direction for measurement of unmatched waveforms. In the measurement of matched (autocorrelation) versus unmatched (cross-correlation) waveforms, our definition of extinction ratio (ER) is the ratio of the autocorrelation peak to the maximum cross-correlation value at any delay. Fig. 2(c) presents the corresponding measured matched (bold solid) correlation trace versus measured unmatched (dashed) correlation trace with an extinction ratio measured as 15.15 dB. For the reverse case in Fig. 2(d), the extinction ratio is observed as 15.35 dB. These agree well with

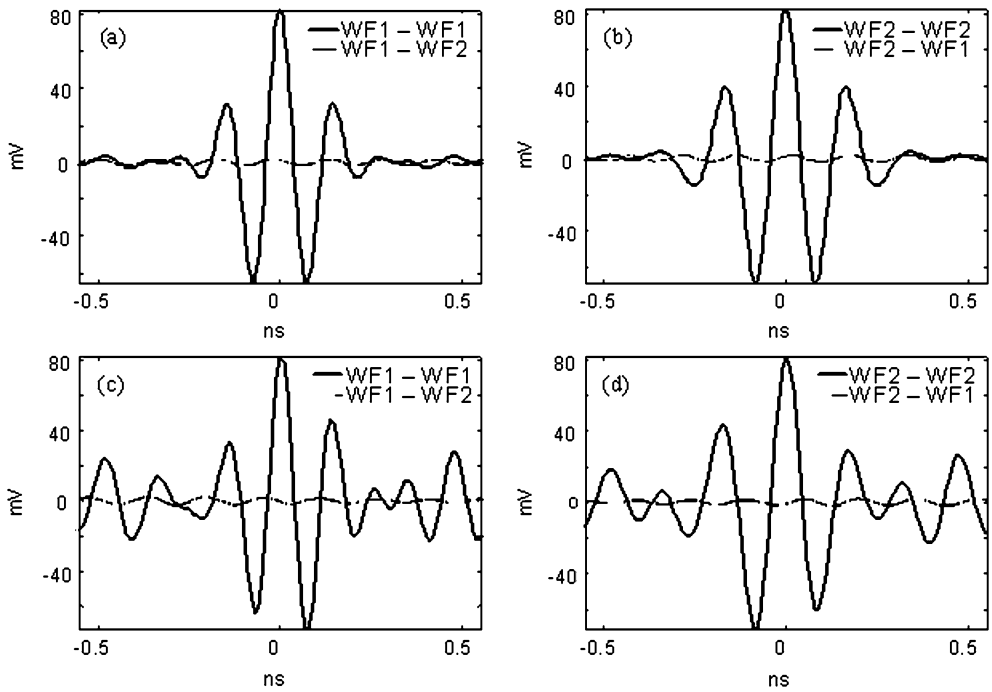

Fig. 3. Simulation of linear chirped waveform correlation traces. WF1 denotes upchirped signal, WF2 denotes downchirped signal. (a) Simulation using ideal waveforms - solid: matched WF1-1, dashed: unmatched WF1-2. (b) Simulation using ideal waveforms - solid: matched WF2-2, dashed: unmatched WF2-1. (c) Simulation using actual measured waveforms - solid: matched WF1-1, dashed: unmatched WF1-2. (d) Simulation using actual measured waveforms- solid: matched WF2-2, dashed: unmatched WF2-1.

the simulated extinction ratios which are discussed next. No low-pass filter was used for our mixer lock-in correlation measurements since the lock-in amplifier already provides a long integration time.

In our simulations of the auto/cross correlation, both ideal and measured linear chirped waveforms are considered with 5–ns integration time. The bandpass characteristics of mixer input ports are included in the calculation with measured cutoff frequencies at 3.7 and 22 GHz. The linear chirped waveform expression can be written in a cosine form as $\mathrm{A(t)}\cdot\cos(0.5\cdot\mathrm{C}\cdot\mathrm{t}^2+\omega_c\cdot\mathrm{t})$, where C is the chirping rate and ω_c is the angular center frequency. In the experiments, we use a numerical value of 15 GHz^2 for the chirping rate (with t in ns) and 6.5 GHz as the center frequency. A(t) is a slowly varying amplitude modulation function resulting from the 3-ns time aperture of our apparatus and the nonuniformity of the input optical power spectrum. Overall this yields the experimental RF power spectrum specified above. Fig. 3 shows the simulated correlation of linear chirped waveforms. WFi - WFj means shaper #1 produces WFi signal and shaper #2 generates WFj signal where $\{i, j = 1 \text{ or } 2\}$. In Fig. 3, WF1 denotes downchirped waveform and WF2 denotes upchirped waveforms. The bold solid lines represent autocorrelation (matched case) with the same sign of input chirps while the dashed line is cross correlation (unmatched case) with opposite signs of input chirps. In Fig. 3(a)–(b), ideal waveforms (computer generated using the cosine formula elaborated above and apodized by the optical input spectrum) are used. In this situation, two ideal input waveforms are aligned perfectly and, therefore, give fast reduction of correlation sidelobes. The extinction ratio defined as the ratio of autocorrelation main peak value to the maximum value of cross correlation is 16.31 dB for both Fig. 3(a) and (b). On the other hand, we also study correlation calculations using the actual measured waveforms from Fig. 2(a) and (b). The resulting simulated correlations are shown in Fig. 3(c)–(d). Now the simulated autocorrelations are no longer perfectly symmetric, since the autocorrelations are obtained from two waveforms that are slightly different since they are generated in different pulse shapers. The simulated correlations using the actual waveforms have slightly larger sidelobes and slightly reduced extinction ratios of 15.38 dB for Fig. 3(c) and 15.84 dB for Fig. 3(d), respectively. These values are quite close to the experimental values, indicating that the mixer operation is close to the ideal multiply and low-pass filter function needed for implementation of the correlation function.

To illustrate the possibility of real-time correlation operation, we also connected the mixer output to a low-pass filter (LPF) with cut-off frequency of 320 MHz and measured the filter output directly on an oscilloscope, as depicted in Fig. 1(a). The same linearly chirped input signals are used as in Fig. 2(a)–(b), and the relative delay is set to zero. No lock-in amplifier is used, and once the delay is set, the delay line plays no further role in this measurement. The filter bandwidth was selected so that its corresponding integration time approximately matches the 3 ns time aperture of the shaped RF waveforms. From the traces in Fig. 4, we clearly observe strong discrimination between matched and unmatched correlation signals. The extinction ratio is $\sim$9 dB at zero delay [highlighted by the vertical dashed line in Fig. 4(b)] and is even stronger in Fig. 4(a) where the cross correlation value is negative at zero delay. The signal to noise demonstrated here, without any signal averaging, should be sufficient for high quality operation when used at the front end of a decision circuit.

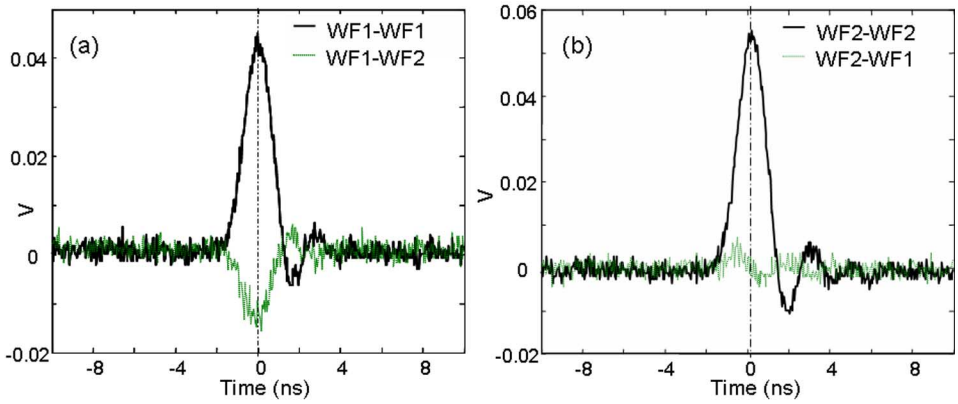

Fig. 4. Linear chirped scope traces of mixer output. (a) Solid: matched WF1-WF1, black-dotted: unmatched: WF1-WF2. (b) Solid: matched WF2-WF2, black-dotted: unmatched: WF2-WF1.

In another example, we use a pair of orthogonal signals designed by the following method. We self-correlated a uniform distributed random sequence generated by the Matlab function RAND, which produces a vector with random entries each chosen from a uniform distribution on the interval (0.0, 1.0). A code length of 8 is used to map onto 64 LCM pixel numbers at 8 pixels per code element. The autocorrelation is performed for different random waveforms until a clear autocorrelation peak with small side lobes is observed. We save and denote this sequence as our sequence #1 and repeat this step to find our next sequence denoted as #2. Then we apply the Gram-Schmidts (GS) procedure [16] to orthogonalize these two sequences at zero delay (after their dc values are subtracted off). Fig. 5(a) shows the generated RF temporal waveforms of sequence #1 produced by two pulse shapers programmed separately, whereas Fig. 5(b) shows sequence #2. The decay at the trailing edge of the temporal waveforms from the first shaper is attributed to the response of an RF amplifier.

Fig. 5(c)–(d) demonstrates a complete set of autocorrelation and cross-correlation measurements, for which we again employ the lock-in amplifier and delay line apparatus of Fig. 1(b). In the solid line of Fig. 5(c), both shapers generate sequence #1; the IF output of the mixer, measured by the lock-in as a function of relative delay, gives rise to an autocorrelation trace with a matched peak in the center and relatively small side-lobes. However, in dash line of Fig. 5(c) the second shaper generates sequence #2 while the first shaper remains the same; the mixer and lock-in output as a function of delay result in a cross-correlation trace. As expected, the cross correlations are very small at zero delay due to the GS orthogonalization procedure. Interestingly, however, the amplitude of the cross–correlation signal remains small over the entire delay range. This reflects the use of different random codes, which are expected to have relatively low correlation even without orthogonalization. Here high–pass filtering at the mixer input may also contribute. In the same manner, the solid line in Fig. 5(d) is taken when both shapers produce sequence #2 and again gives an obvious autocorrelation trace, while for the dashed line the second shaper generates sequence #1 and the first shaper remains at sequence #2, which provides the cross-correlation trace. The nonsymmetric sidelobes of autocorrelation traces are due to the slightly non-identical shape of waveforms produced from pulse shapers and the frequency dependence of mixer response. Here, we observed measured extinction ratios of 15.68 dB for the data shown in Fig. 5(c) and 14.19 dB for another case in Fig. 5(d). Simulations (not shown) were also performed for the orthogonal sequences. For the orthogonal signal sets, the calculated extinction ratio is 15.95 dB for the ideal (design) waveforms. By using the actual measured waveforms in the simulation, the calculated extinction ratios become 15.79 dB (WF1- WF1 versus WF1- WF2) and 14.24 dB (WF2- WF2 versus WF2- WF1). These results are again close to the experimental values.

IV. Correlation Detection Over Wireless Link

We also explore the possibility of correlation detection over a broadband wireless link, which is built by a pair of UWB RF horn antennas (Dorado Inc. model# GH 1–12 N) with operational range 1–12 GHz and coaxial input ports.

These commercial horn antennas exhibit strong dispersion at low frequencies below 2 GHz but are mostly dispersionless at higher frequencies [17]. One homemade high-pass filter (HPF) is inserted at the transmitter to eliminate low frequency components below 1 GHz that are particularly susceptible to antenna dispersion. We place our pulse shaper #1 in the transmitter to generate the RF signals, and pulse shaper #2 in the receiver to produce LO signals. A third RF amplifier is inserted right after the UWB receive antenna to enhance the captured signal prior to the mixer. A complete setup is shown in Fig. 6. Currently the laser pulses share one 5.5–km single-mode fiber stretcher and then an optical splitter is used after the fiber. The height of both UWB antennas is $\sim$1 m and the separation between the antennas is $\sim$1 m to ensure far-field operation. The antennas are arranged for line-of-sight operation (LOS). Fig. 7 shows the linear chirped waveforms after wireless transmission. The original transmitted data is an upchirped signal which gives a time-domain waveform from the receive antenna [Fig. 7(a)] with late-time ripples (dashed circle) beyond $\sim$1.5 ns arising from the antenna dispersion. Since a HPF is inserted prior to the transmitting antenna, and since the wireless transmission itself cuts out the baseband, all received signals are bipolar. In order

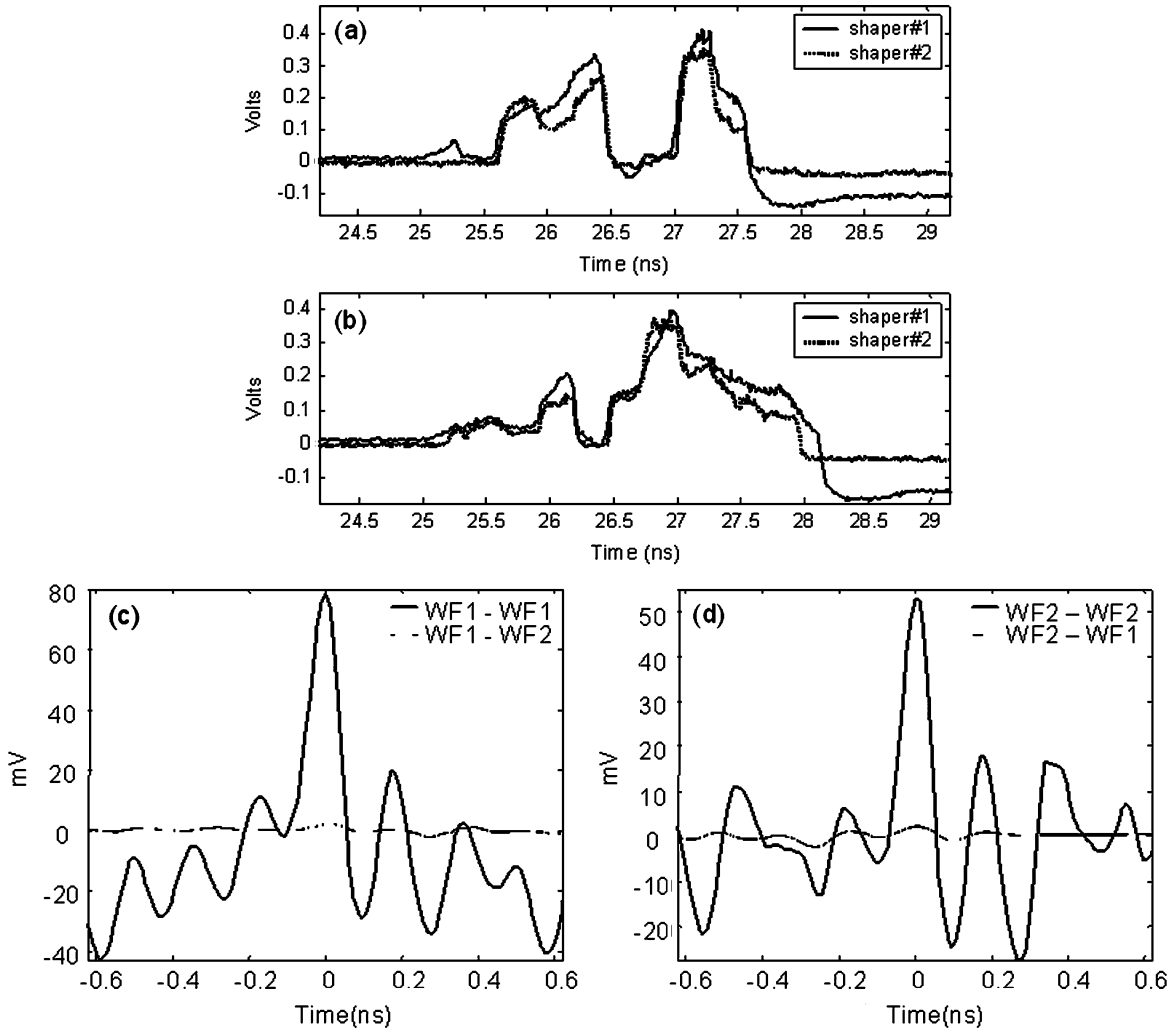

Fig. 5. Temporal waveforms of user-defined orthogonal signals. (a) Sequence #1 (b) sequence #2; Correlation traces. (c) Solid: matched WF1-WF1, dashed: unmatched WF1-WF2. (d) Solid: matched WF2-WF2, dashed: unmatched WF2-WF1.

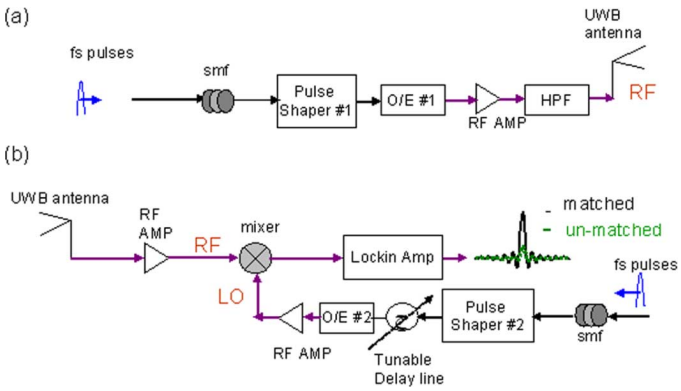

Fig. 6. UWB wireless correlation detection setup. (a) RF transmitter. (b) Heterodyne receiver with local oscillator; Purple lines indicate RF cables, and black lines are optical fibers. The femtosecond pulses are produced from one fiber laser and sent into the same fiber strecher (SMF). The pulses are then split by a 3–dB optical splitter prior to the pulse shapers.

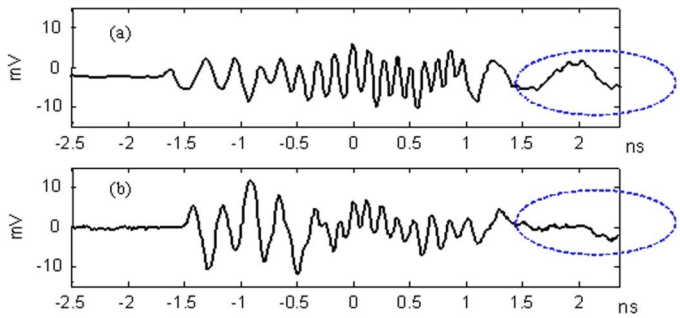

Fig. 7. Wireless transmission of linear chirped signals. (a) Antenna received signal. (b) Antenna received precompensated signal.

to precompensate the dispersion of the antenna link, we apply the phase conjugate of the antenna wireless channel frequency response to the drive waveform [9]. The frequency response of the antennas and line-of-sight wireless channel is obtained by driving the transmit antenna with a short ($\sim$40 ps) pulse and measuring the output from the receive antenna on a sampling oscilloscope, which approximates the impulse response. When the upchirped drive signal is predistorted in order to compensate dispersion, the late-time ripples in the received signal are suppressed, as seen in Fig. 7(b) (dashed circle). Similar operation can be achieved by postcompensating the LO signal (from shaper #2), making use of the same channel information.

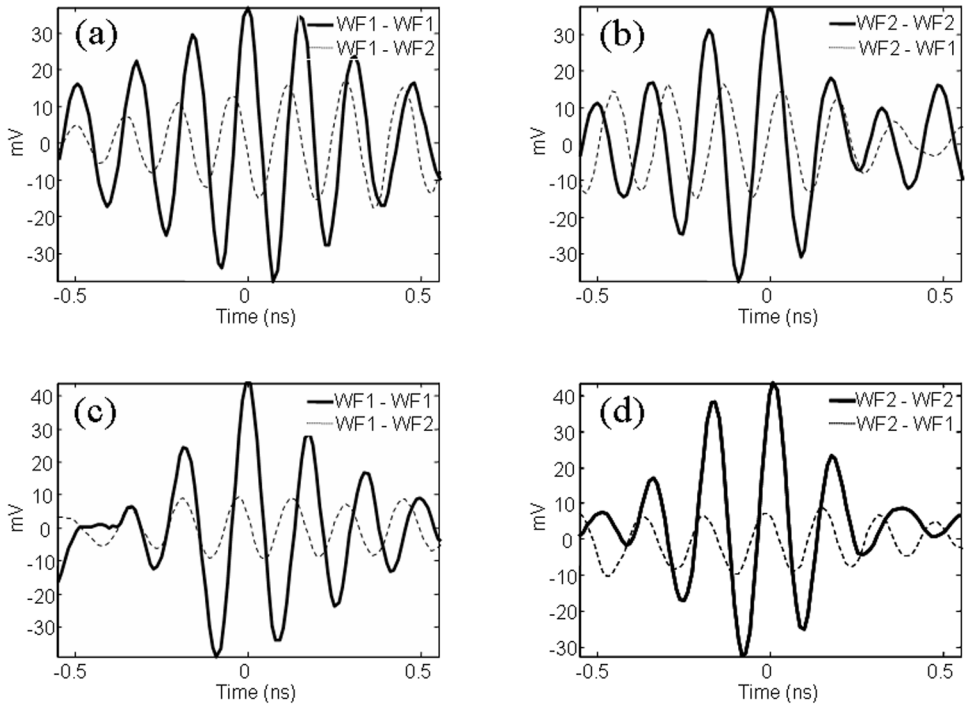

Fig. 8. Measurement of wireless correlation detection of linear chirped signals (a)-(b) without any waveform compensation. (c)-(d) With RF waveform precompensation.

The correlation measurements performed after the short wireless link are shown in Fig. 8. For the experiment without dispersion precompensation, we observe a significantly larger cross correlation. The measured extinction ratio is 3.41 dB for Fig. 8(a) and 3.58 dB for Fig. 8(b), respectively. Improved results are obtained when using UWB dispersion precompensation. The resulting correlation measurements are shown in Fig. 8(c)–(d). The cross correlations become smaller and the roll-off of the autocorrelation sidelobe becomes faster as well. The measured extinction ratios are also boosted to 6.84 dB [Fig. 8(c)] and 7.10 dB [Fig. 8(d)] with aid of dispersion precompensation. Note that though improved, these contrasts are still below what was obtained for the linear chirped waveforms without the free-space link. One reasons for this lies in a reduction in bandwidth due to frequency-dependent transmission in the wireless link. This is evident as a lengthening of the autocorrelation traces in Fig. 8 compared to those in Fig. 2. From the Fourier transform of the autocorrelation data, we estimate that the 3-dB widths of the power spectra are narrowed by 13.4% after transmission over the antenna link.

V. Conclusion

We have described electrical correlation measurements of photonically generated UWB RF waveforms. Our measurements demonstrate significant waveform selectivity, with ∼15 dB contrast between correlations performed with matched waveform pairs compared to nonmatched waveforms. We have also demonstrated the potential for real-time detection and have extended our experiments to include transmission over a short line-of-sight wireless link. Photonic techniques for generation and correlation processing of UWB RF waveforms may serve as enablers for novel wireless UWB schemes including laboratory tests of wireless UWB-CDMA, which have recently been theoretically analyzed [13] but not been implemented due to lack of waveform generation and processing hardware capable of covering a large fraction of the UWB band.

Acknowledgment

The authors would like to thank Dr. J. McKinney for valuable discussions, and also Prof. Chappell's group at Purdue University for their help in RF high-pass filter fabrication.

References

[1] M. Z. Win and R. A. Scholtz, "Ultra-wide bandwidth time-hopping spread-spectrum impulse radio for wireless multiple-access communications," *IEEE Trans. Commun.*, vol. 48, no. 4, pp. 679–691, Apr. 2000.

[2] J. D. McKinney, D. E. Leaird, and A. M. Weiner, "Millimeter-wave arbitrary waveform generation with a direct space-to-time pulse shaper," *Opt. Lett.*, vol. 27, no. 15, pp. 1345–1347, Aug. 2002.

[3] I. S. Lin, J. D. McKinney, and A. M. Weiner, "Microwave arbitrary waveform generation with applications in ultra-wideband comm.," *IEEE Microw. Wireless Compon. Lett.*, vol. 15, no. 4, pp. 226–228, 2005.

[4] J. D. McKinney, I. S. Lin, and A. M. Weiner, "Shaping the power spectrum of ultra-wideband radio-frequency signals," *IEEE Trans. Microw. Theory Tech.*, vol. 54, no. 12, pp. 4247–4255, Dec. 2006.

[5] J. Chou, Y. Han, and B. Jalali, "Adaptive RF-photonic arbitrary waveform generator," *IEEE Photon. Technol. Lett.*, vol. 15, no. 4, pp. 581–583, 2003.

[6] C. Wang, F. Zeng, and J. Yao, "All-fiber ultrawideband pulse generation based on spectral shaping and dispersion-induced frequency-to-time conversion," *IEEE Photon. Technol. Lett.*, vol. 19, no. 3, 2007.

[7] M. Abtahi, M. Mirshafiei, J. Magne, L. A. Rusch, and S. LaRochelle, "Ultra-wideband waveform generator based on optical pulse-shaping and FBG tuning," *IEEE Photon. Technol. Lett.*, vol. 20, no. 2, pp. 135–137, 2008.

[8] [Online]. Available: http://www.tek.com/products/signal_sources/awg7000/index.html

[9] J. D. McKinney and A. M. Weiner, "Compensation of the effects of antenna dispersion on UWB waveforms via optical pulse-shaping techniques," *IEEE Trans. Microw. Theory Tech.*, vol. 54, no. 4, pt. 2, pp. 1681–1686, June 2006.
[10] D. Gallagher and D. Malocha, "Orthogonal frequency coding for use in ultra wide band communications and correlators," in *Proc. IEEE Freq. Control Symp.*, 2006.
[11] S. Y. Ng, B. Jalali, P. Zhang, J. Wilson, and I. Mohammad, "A low voltage CMOS 5-bit 600 MHz 30 mW sar adc for UWB wireless receivers," in *Proc. 48th Midwest Symp. Circuits Syst.*, 2005, pp. 187–190.
[12] R. Brocato, J. Skinner, G. Wouters, J. Wendt, E. Heller, and J. Blaich, "Ultra-wideband SAW correlator," *IEEE Trans. Ultrason., Ferroelectr. Freq. Control*, vol. 53, no. 9, pp. 1554–1556, Sep. 2006.
[13] M. Farhang and J. A. Salehi, "Spread-time/time-hopping UWB CDMA communication," in *Proc. IEEE Symp. Commun. Inf. Technol.*, 2004, vol. 2, pp. 1047–1050.
[14] I. S. Lin and A. M. Weiner, "Hardware correlation of ultra-wideband RF signals generated via optical pulse shaping," in *Proc. IEEE Int. Top. Meet. Microw. Photon.*, Victoria, Canada, Oct. 2007, pp. 149–152.
[15] S. Xiao and A. M. Weiner, "Programmable photonic microwave filters with arbitrary ultra-wideband phase response," *IEEE Trans. Microw. Theory Tech.*, vol. 54, no. 11, pp. 4002–4008, Nov. 2006.
[16] J. G. Proakis, *Digital Communications*, 4th ed. New York: McGraw-Hill, 2001.
[17] J. D. McKinney, D. Peroulis, and A. M. Weiner, "Time-Domain Measurement of the Frequency-Dependent delay of Broadband Antennas," *IEEE Trans. Antennas Propag.*, vol. 56, no. 1, pt. 2, pp. 39–47, Jan. 2008.

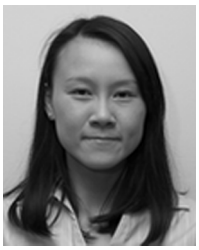

Ingrid S. Lin (S'02) received the B.S. degree (with highest honors) in communication engineering from National Chiao-Tung University, Hsinchu, Taiwan, R.O.C., in 2002.

She is currently working toward the Ph.D. degree at Purdue University, West Lafayette, IN. She received a Graduate Fellowship (supported by General Electric) from Purdue University, where she is currently a Research Assistant with the School of Electrical and Computer Engineering. Her research interest is in ultrafast optics focusing on optical pulse shaping, arbitrary waveform generation, and RF photonics with applications in ultrawide bandwidth communication. She has authored or coauthored three journal papers and 12 conference papers.

Ms. Lin is a member of the IEEE Lasers and Electro-Optics Society. She was listed in the National Science Foundation (NSF) Graduate Fellowship Honorable Mentions in 2003. She was also a recipient of the Graduate Assistance in Areas of National Need (GAANN) Fellowship (2003–2006).

Andrew M. Weiner (F'95) received the Sc.D. degree in electrical engineering from the Massachusetts Institute of Technology (MIT), Cambridge, in 1984.

From 1979 to 1984, he was a Fannie and John Hertz Foundation Graduate Fellow with MIT. Upon graduation, he joined Bellcore, first as Member of Technical Staff and later as Manager of Ultrafast Optics and Optical Signal Processing Research. He moved to Purdue University, West Lafayette, IN, in 1992 and is currently the Scifres Distinguished Professor of Electrical and Computer Engineering. His research focuses on ultrafast optics signal processing and applications to high-speed optical communications and ultrawideband wireless. He is especially well known for his pioneering work in the field of femtosecond pulse shaping. He has published six book chapters and more than 200 journal articles. He has been the author or coauthor of more than 350 conference papers, including approximately 80 conference invited talks, and has presented nearly 100 additional invited seminars at university, industry, and government organizations. He holds 10 U.S. patents.

Prof. Weiner is a Fellow of the Optical Society of America. He was the recipient of numerous awards for his research, including the Hertz Foundation Doctoral Thesis Prize (1984), the Adolph Lomb Medal of the Optical Society of America (1990), awarded for pioneering contributions to the field of optics made before age 30, the Curtis McGraw Research Award of the American Society of Engineering Education (1997), the International Commission on Optics Prize (1997), the IEEE LEOS William Streifer Scientific Achievement Award (1999), the Alexander von Humboldt Foundation Research Award for Senior U.S. Scientists (2000), and the OSA R.W. Wood Prize (2008). He has been recognized by Purdue University with the inaugural Research Excellence Award from the Schools of Engineering (2003) and with the Provost's Outstanding Graduate Student Mentor Award (2008).